Article

A Fluorescent Chemodosimeter for Organelle-Specific Imaging of Nucleoside Polyphosphate Dynamics in Living Cells

Harwinder Singh, Sreejesh Sreedharan, Rajeshwari Tiwari, Christa. Walther, Carl G W Smythe, Sumit Pramanik, Jim Antony Thomas, and Amitava Das

Cryst. Growth Des., **Just Accepted Manuscript** • DOI: 10.1021/acs.cgd.8b01409 • Publication Date (Web): 08 Oct 2018

TOC

A Fluorescent Chemodosimeter for Organelle-Specific Imaging of Nucleoside Polyphosphate Dynamics in Living Cells

Harwinder Singh, Sreejesh Sreedharan, Rajeswari Tiwari, Christa Walther, Carl Smythe, Sumit Kumar Pramanik, Jim. A. Thomas and Amitava Das

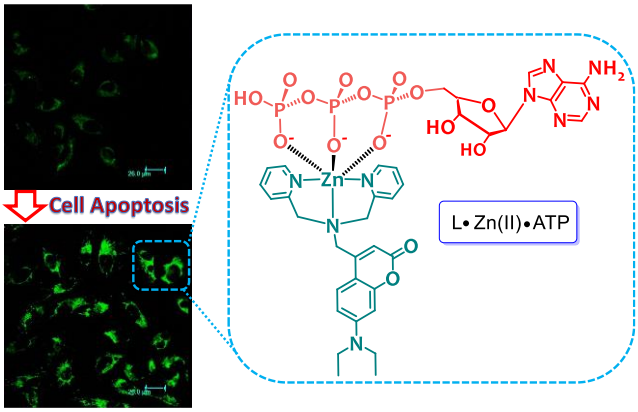

New fluorescence-based reagent for probing subtle changes of NPPs in mitochondria

A Fluorescent Chemodosimeter for Organelle-Specific Imaging of Nucleoside Polyphosphate Dynamics in Living Cells

Harwinder Singh,[a] Sreejesh Sreedharan,[b,c] Rajeswari Tiwari,[a] Christa Walther,[d] Carl Smythe,[e] Sumit Kumar Pramanik,[a*] Jim. A. Thomas[b*] and Amitava Das[a*]

[a] CSIR-Central Salt & Marine Chemicals Research Institute, Bhavnagar: 364002, Gujarat, India; E-Mail: sumitpramanik@csmcri.res.in (SKP); a.das@csmcri.res.in (AD)

[b] Current address: CRUK/MRC Oxford Institute for Radiation Oncology, Department of Oncology, University of Oxford, Oxford OX3 7DQ, UK

[c] Department of Chemistry, University of Sheffield, Sheffield, S3 7HF, UK, Email: james.thomas@sheffield.ac.uk.

[d] Molecular Biology and Biotechnology, University of Sheffield, Sheffield, S3 7HF, UK.

[e] Department of Biomedical Science, University of Sheffield, Sheffield, S10 2TN, UK.

ABSTRACT

Nucleoside polyphosphates (NPPs) are mainly produced in mitochondria and used as a universal energy source for various cellular events. Although numerous fluorescent probes for Adenosine Tri-Phosphate (ATP) have been reported, they are not ideally suited for live monitoring of the subtle variation of mitochondrial ATP level. A new coumarin-based fluorescent probe is synthesized and this reagent is utilized for specific recognition of NPPs in mitochondria by super resolution microscopy in physiological condition. Detailed ^{31}P NMR studies reveal that the probe, L●Zn(II), binds to NPPs through their pendent phosphate functionalities. Such binding leads to a substantial enhancement in the luminescence intensity of L●Zn(II)+ADP or L●Zn(II)+ATP as compared to L●Zn(II). This - as well as ^{1}H NMR spectroscopy - has enabled us to evaluate the probe's binding affinities to these NPPs. Structured illumination and wide field fluorescence microscopy confirmed that this physiologically benign reagent is localized within mitochondria of live RAW 264.7 macrophage cells. This reagent has been utilized to probe real-time changes in ATP concentrations within mitochondria during drug-induced apoptosis.

1. INTRODUCTION

Nucleoside polyphosphates (NPPs) are considered to be the main energy vectors of the cell and play pivotal roles in various cellular events.[1-2] The most familiar NPP, Adenosine Tri-Phosphate (ATP) is seen as the primary energy currency. It is largely produced in mitochondria and regulates cellular metabolism.[3] ATP is an important marker for studying cell injury, tumor progression/ cancers and many critical diseases. [3-4] In addition, NPPs are crucial for intracellular and extracellular signaling process.[2] In mammalian tissues, the release of NPPs from synapses and axons activates purinergic receptors, which modulate intracellular calcium and cyclic AMP levels.[5-6] In the central nervous system, ATP modulates neural development, the control of immune systems, and neuron/glial signaling.[5, 7] NPPs are also involved in signal transduction as their phosphate groups are used as substrates for kinases in phosphate transfer reactions which activate a cascade of protein kinase reactions. [8-9] Besides these intracellular roles, NPPs are extracellularly controlled by various chemical and mechanical stimuli. [10-12] Thus, intracellular ATP concentrations quickly vary in response to a wide variety of external stimuli, including cytotoxic agents, nutrients, hypoxia, and hormones.

In eukaryotic cells, ATP is mostly synthesized during glucose metabolism in mitochondria through oxidative phosphorylation. [13-14] During the transfer of hydrogen atoms from $FMNH_2$ or $FADH_2$ to oxygen, protons are pumped across the mitochondrial membrane from the inside of the mitochondrion to the outside. [15-17] This creates an electrical potential across the mitochondrial membrane, corresponding to 200-300 millivolts, and it is this electrical energy that is converted into chemical energy by ATP synthase enzyme, generating ATP from ADP. [17] Alterations of mitochondrial membrane potential in eukaryotic cells leads to mitochondrial dysfunction and this appears as a common phenotype in mitochondrial diseases affecting ATP production. [17]

Therefore, methods to specifically detect and quantify ATP are extremely important. It has been argued that subtle variations in the concentration of NPPs within mitochondria are also indicative of various disease conditions. [3-4, 18] Thus, a highly sensitive, specific and quantitative detection platform for the real-time monitoring of NPPs is a highly attractive goal within the context of clinical diagnostic. Whilst, various detection methods for NPPs have been reported, [19-23] fluorescent probe that localizes in the mitochondrion are highly suited for this application, as such reagents allows selective monitoring of biological events as they occur inside this organelle.[18, 24-27] Hence, the synthesis of organelle-specific molecular probes that produce a luminescence ON response on binding to, or reacting with, NPPs would have significance for clinical diagnosis, cell biology and assessing analytical samples. Yet contemporary literature reports on fluorescent chemodosimeters that are proficient in analyzing the spatial and temporal dynamics of NPPs in mitochondria are rare.

Conventional fluorescence microscopy allows non-invasive imaging of lysosomes and mitochondria in live cells.[28] However, it suffers from an optical diffraction-limited spatial resolution and fails in resolving the membrane boundaries between lysosomes and mitochondria.[28] Although electron microscopy can overcome this limitation, it fails in capturing dynamic processes in live cells. More recently many of the drawbacks of conventional imaging modalities have been addressed through super-resolution microscopy (SRM) techniques, which can overcome the diffraction limit of conventional optical but can still be employed to monitor dynamic processes. One such SRM technique is SIM (structured illumination microscopy), which provides an appreciable increase in resolutions (to 100–120 nm) with negligible disruption of data acquisition rate. [29-30] SIM requires considerably lower illumination intensities compared to other super-resolution microscopies like STORM and STED, making it particularly suited for live cell imaging. [30-32] However, most existing mitochondrial probes undergo photo-bleaching under SIM.[33]

In this manuscript, we report a turn-on luminescent probe for NPPs that spontaneously localizes in mitochondria, without anchor-protein expression. Taking advantage of its ability for selective subcellular internalization, this chemodosimetric probe has been successfully used to image the subtle changes in the effective concentration of NPPs within living cells at super-resolutions. This has allowed us to detect the extracellular release of NPP from living cells and observe stimuli-responsive change in ATP concentration in mitochondria. To the best of our knowledge, this probe provides unique capabilities for the visualization of NPPs dynamics in the mitochondria of live cells, along with simultaneous detection of changes in ATP concentration within cellular compartments using multicolor imaging.

2. EXPERIMENTS AND METHODS

Materials.

All common chemicals and solvents were procured from commercial suppliers and used without any further purification unless mentioned otherwise. 7-Diethylamino-4-methylcoumarin (99.0%), dichloromethane (DCM) (> 99.0%), Selenium dioxide (> 99.0%), Methanesulfonyl chloride (99%), Sodium borohydride (98%), Zinc perchlorate hexahydrate, Di-(2-picolyl)amine (DPA), Xylene (> 99.0%), Lithium bromide (> 99.0%), phosphate buffer saline (PBS), fetal bovine serum, penicillin−streptomycin, 4% paraformaldehyde (PFA), Vectashield h-1000 (mounting agent), 50 mM ammonium chloride, Lyso tracker red, Mito tracker deep red, and Hoechst (33342) were purchased from Sigma-Aldrich. Iscove's Modified Dulbecco's Medium (IMDM), fetal calf serum (FCS), Dulbecco's Modified Eagle's medium (DMEM), Alexa Fluor 488 Donkey Anti-Mouse IgG (H+L) antibody, mouse monoclonal anti-α-tubulin antibody, and 4′,6-Diamidino-2-Phenylindole (DAPI) were purchased from Life Technologies. The 15 μ-slide 8 wells were purchased at Ibidi. The culture plates and dark plates

were obtained from Greiner Bio One. RAW 264.7 macrophage cell line was purchased from ATCC.

Synthesis of the probe L•Zn(II).

To a solution of **3** (0.277 g, 1.12 mmol) in anhydrous CH_2Cl_2, methanesulfonyl chloride (0.13 mL, 1.68 mmol) was added at 0° C. After **3** was consumed (as determined by TLC), saturated $NaHCO_3$ solution (20 mL) was added. The aqueous phase was extracted with CH_2Cl_2 (3 × 50 mL) and the combined organic phases were dried and concentrated. The obtained crude product was immediately dissolved in anhydrous THF (10 mL). Anhydrous lithium bromide (0.292 g, 3.36 mmol) was added to the solution and the mixture was stirred at room temperature for 1 hour. The solvent was evaporated and the crude product was purified by column chromatography (PE/EA = 2.5:1) to afford product **4** as orange crystals (0.285 g, Yield: 82 %). **^{1}H NMR** (600 MHz, $CDCl_3$): δ 1.18 (6H, t, *J* = 6.0 Hz), 3.39 (4H, q, *J* = 6.0 Hz), 4.37 (2H, s); 6.10 (1H, s); 6.48 (1H, s), 6.59 (1H, d, *J* = 12.0 Hz); 7.46 (1H, d, *J* = 12.0 Hz). **^{13}C NMR** (150 MHz, $CDCl_3$): δ 12.43, 27.08, 44.86, 97.86, 106.04, 108.75, 109.14, 125.29, 150.23, 151.03, 156.73, 161.77.

To a round-bottom flask equipped with a stir bar was charged with **4** (0.168 g, 0.56 mmol), Di-(2-picolyl)amine (0.1 mL, 0.56 mmol) and Na_2CO_3 (0.350 g, 3.33 mmol). Then, CH_2Cl_2 (20 mL) was added. The reaction mixture was stirred at 140 ^{o}C for 24 h until purine was consumed (determined by TLC). Then, the solvent was removed and purified by column chromatography on silica gel (PE/ 85% EtOAc followed by CH_2Cl_2/5% MeOH) to afford **L** as light yellow solid (0.211 g, Yield: 91 %).

^{1}H NMR (600 MHz, $CDCl_3$): δ 1.20 (6H, t, *J* = 6.0 Hz); 3.4 (4H, q, *J* = 6.0 Hz); 3.82 (2H, s); 3.90 (2H, s); 6.48 (1H, s), 6.49 (1H, d, *J* = 6.0 Hz), 6.54 (1H, d, *J* = 12.0 Hz); 7.18 (2H, t, *J* = 6.0 Hz); 7.47 (1H, d, J = 12.0 Hz); 7.54 (2H, d, *J* = 6.0 Hz) 7.68 (2H, t, *J* = 6.0 Hz), 8.54 (2H,

d, J = 6.0 Hz). **^{13}C NMR** (150 MHz, $CDCl_3$): δ 12.41, 44.90, 54.25, 60.74, 97.83, 107.79, 108.16, 122.30, 123.06, 125.26, 136.77, 148.99, 150.32, 153.75, 156.33, 158.51, 162.48.

A round-bottom flask equipped with a stir bar was charged with **1** (1.0 g, 4.32 mmol), and SeO_2 (0.958 g, 8.64 mmol). Then, xylene (20 mL) was added. The reaction mixture was stirred at room temperature for 24 h until **1** was completely consumed (determined by TLC). Then the reaction was filtered and the organic phase was concentrated. The obtained crude product (**2**) was immediately dissolved in ethanol (200 mL) and anhydrous sodium borohydride (0.49 g, 12.96 mmol) was added and the mixture was stirred at room temperature for 12 hour. Then, the solvent was removed and purified by column chromatography on silica gel (PE: EtOAc is 1:1) to afford **3** as yellow solid (0.765 g, Yield: 72 %).

^{1}H NMR (600 MHz, $CDCl_3$): δ 1.19 (6H, t, *J* = 6.0 Hz), 3.39 (4H, q, *J* = 6.0 Hz), 4.82 (2H, s); 6.27 (1H, s); 6.47 (1H, s); 6.55 (1H, d, *J* = 12.0 Hz); 7.30 (1H, d, *J* = 6.0 Hz). **^{13}C NMR** (150 MHz, $CDCl_3$): δ 12.29, 44.62, 60.48, 97.62, 105.21, 106.22, 108.81, 124.48, 150.20, 155.23, 156.15, 163.03.

To a solution of **L** (0.500 g, 1.03 mmol) in MeOH, $Zn(ClO_4)_2$, $6H_2O$ (0.521 g, 1.4 mmol, in 10 mL HPLC water) was added in a drop wise manner. The resultant solution mixture was allowed to stir for 6 h at 20 ^{o}C. A yellow coloured precipitate appeared, which was filtered off and dried in air to obtain the **L•Zn(II)** complex in a pure form (0.523 g. Yield: 90%).

^{1}H NMR (600 MHz, DMSO-d_6): δ 8.45(2H, d, *J*= 4.0 Hz), 7.77 (2H, t, *J* = 4.0Hz), 7,58 (2H, d, *J* = 4.0), 7.54 (1H, d, *J* = 8.0 Hz), 7.27 (2H, t, *J* = 4.0 Hz), 6.64 (1H, d, *J* = 8.0 Hz), 6.42 (1H, s), 6.29 (1H, s), 3.89 (4H, s), 3.84 (2H, s), 3.43 (4H, d, *J* = 4.0 Hz), 1.17 (6H, t, *J* = 4.0 Hz). **^{13}C NMR** ($CDCl_3$, 125 MHz): 160.92, 155.86, 154.61, 151.14, 148.04, 141.19, 126.23, 125.37, 111.36, 109.25, 108.42, 97.69, 57.00, 44.43, 12.91.

Cell Culture

RAW 264.7 macrophage cell line were incubated in DMEM supplemented with 10% (v/v) fetal bovine serum and 1% (w/v) penicillin-streptomycin at 37 °C in presence of 5% of CO_2 in the humidified air. Cells were passaged when they are approximately 80% confluence. Then the cells were seeded onto a cell culture dish at a density of 1.0×10^5 cells incubated at 37 °C under 5% CO_2 in the humidified air.

MTT Assay

Initially, the molecular probe L•Zn(II) was tested for cytotoxicity towards RAW 264.7 macrophage cell line. RAW 264.7 macrophage cell were placed in a 96 well plated at a density of 1.0×10^5 cells/well in DMEM medium (Gibco), supplemented with 5% fetal bovine serum along with 100 units of penicillin−streptomycin antibiotics. The cells were incubated at 37 °C in a 5 % CO_2 incubator for 24 h after which they were washed with 1 x PBS. A total of six wells per condition were taken and 100 µL were added to the respective wells: blank (supplemented IMDM medium), cell death, 120 µM, 60 µM, 30 µM and 15 µM of probe molecule L•Zn(II) in the supplemented IMDM medium. The cells were left to incubate for 48 h in the incubator after that these cells were washed thrice with 1 x PBS. Then 100 µL of **10%** MTT [3-(4,5-Dimethylthiazol2-yl)-2,5-diphenyltetrazolium bromide] solution, in supplemented IMDM medium, was added to each well and further incubated for another 4 h. Then the solution was transferred to a dark plate and the absorbance measured at 570 nm. Each experiment was performed in triplicate.

Microscopy Experiments

Deconvolution Widefield Microscopy

To remove the out of focus blur from stacks of acquired Z-Stack images, deconvolution of raw widefield images acquired using the OMX-SIM (Conventional Wide Field Microscopy mode) was carried out using the Soft Worx software.

Cellular uptake of L•Zn(II) complex (Single colour Imaging)

Single colour widefield experiments using L•Zn(II) were performed at a range of concentrations (10 μM to 200 μM) of L•Zn(II) and uptake studies were carried out over 24 hours. For single colour widefield experiments, an excitation wavelength of 400 nm was used and luminescence was collected at 500 to 550 nm. The widefield microscopy conditions maintained were; Z stack thickness (Sections 40 to 80), section spacing (0.250 to 0.500), and thickness of the sample (8 to 11). Selected exposure times were between 10 to 30 s and the %T was in the range of 30 to 60.

Colocalization Experiments (Multicolour imaging)

Individual colocalization experiments were performed using LysoTracker Deep Red or Mito Tracker Deep Red. For these colocalization experiments, the RAW 264.7 macrophage cell line were incubated with 50 μM of LZn(II) for 4 hours and then the cells were incubated with LTDR or MTDR (750 nM) for 30 minutes. These pre-treated cells (fixed with 4% PFA and mounted) were washed thrice with DMEM culture media and then thrice with PBS. The L•Zn(II) complex was excited at 400 nm and the emission was collected in the FITC Channel (500 to 550 nm). For these studies, Lyso or Mito Tracker Deep Red or Hoechst was excited at 644 nm and emission was collected in the Alexa Fluor 647 Channel (> 650 nm).

SIM Microscopy - Single colour, Colocalisation, and Dual colour experiments

Structured illumination microscopy (SIM) was carried out by using the Delta Vision OMX-SIM. The Z stacks acquired during the imaging were post-processed by using the reconstruction option of Soft Worx. For single colour experiments, the L•Zn(II) complex was excited at 400 nm and the emission was collected at FITC Channel (500 to 550 nm). The Structured Illumination (SI) experimental condition employed for running the SI experiment for single colour experiments were mainly dependent on the thickness of the Z stack (Sections 80 to 100), section spacing (0.125 to 0.250), the thickness of the sample (8 to 10). The dual colour experiments were performed in combination with Hoechst.

3. RESULTS AND DISCUSSION

We chose coumarin as a luminescence-based reporter functionality due to its excellent photophysical properties, such as high molar absorptivity, excellent photostability, tuneable emission through appropriate derivatization, as well as a relatively narrow emission bandwidth with high luminescence quantum yield. [34-35] The synthesis of L•Zn(II) complex is outlined in Scheme 1. All the characterization data are provided in the supporting information.

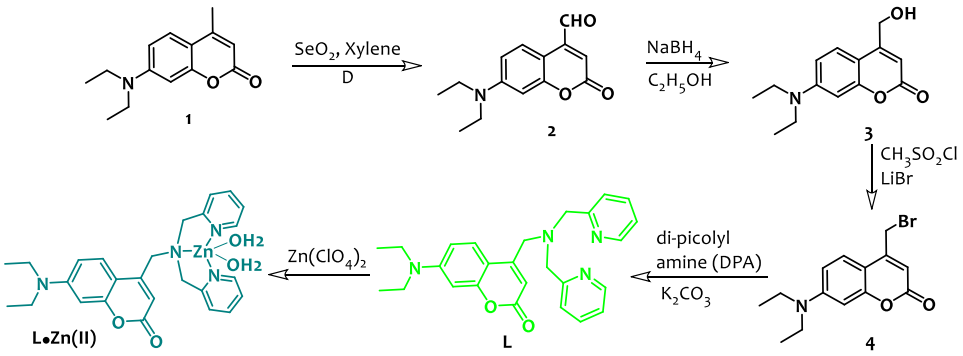

Scheme 1 The synthetic route towards L•Zn(II)complex.

The absorption spectrum of L•Zn(II) was recorded in an aqueous HEPES buffer solution at pH 7.4. A strong absorption band with a maximum at 400 nm (ε = 38000 L mol^{-1} cm^{-1}) was observed and this was attributed to an S_0–S_1 intramolecular charge transfer (ICT) with the amine functionality as the donor and the coumarin moiety as the acceptor fragment. During titration with $Zn(ClO_4)_2$, the luminescence intensity (λ_{Ext} = 400 nm) of ligand **L** was found to decrease slowly and eventually a weak emission band ($\phi_{500nm}^{LZn(II)}$ = 0.0136) with a maximum at 500 nm was observed upon addition of 2 mole equiv. of $Zn(ClO_4)_2$ (Figure S1). Binding of the Zn(II)-centre to the bis picolyl moiety (Scheme 1) would further favor the ICT process and account for a narrower HOMO–LUMO energy gap. The smaller energy gap between frontier orbitals promotes non-radiative deactivation of the excited state and hence, the lowered emission quantum yield of L•Zn(II). The luminescence spectral response of L•Zn(II) towards a variety of anionic analytes was tested using 50-mole equivalents of the respective analytes. No noticeable change in luminescence profile was observed when spectra were recorded in the presence of all other analyte (e.g., X: H_2O_2, OH^-, HNO, Na_2S_2, NO_3^-, NO_2^-, NO_3^-, SO_4^{2-}, SO_3^-, $S_2O_3^-$, Cl^-, urea, PPi, AMP, creatinine and all natural amino acids (AA)), except for NPPs (ADP and ATP) (Figure S2). On treatment with NPPs, a distinct enhancement in luminescence intensity was observed for the luminescence band centered at 500 nm ($\phi_{500nm}^{LZn(II)-ATP}$ = 0.341 and $\phi_{500nm}^{LZn(II)-ADP}$ = 0.337 for λ_{Ex} = 400 nm; coumarin was used as a standard to estimate relative emission quantum yields).

These observations are consistent with other reports showing that Zn(II) systems have an affinity towards ATP and ADP; [22, 36] for example, the Zn(II)-centre in Zn(DPA) or Zn(cyclam) bind to ATP and/or ADP through their pendent phosphate moieties (Figure 1). [21, 37-40]

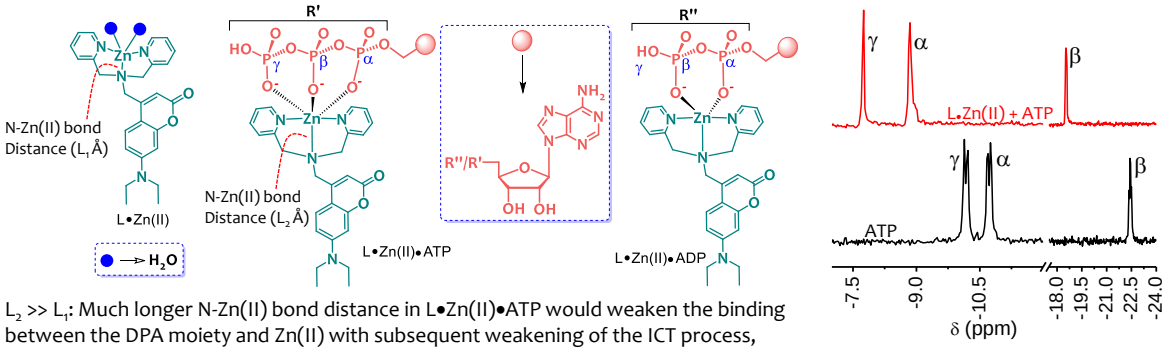

Figure 1. (a) Molecular structure showing the probable binding of ATP and ADP to L•Zn(II) and (b) partial ^{31}P NMR spectra of ATP and ATP bound to L•Zn(II).

This possibility for L•Zn(II). was confirmed from the results of the P^{31} NMR studies (*vide infra*). This binding is expected to decrease the interaction between the DPA moiety and Zn(II) and subsequent weaken the ICT process, which is otherwise operational in the complex. This effect contributes to the observed enhanced luminescence intensity.

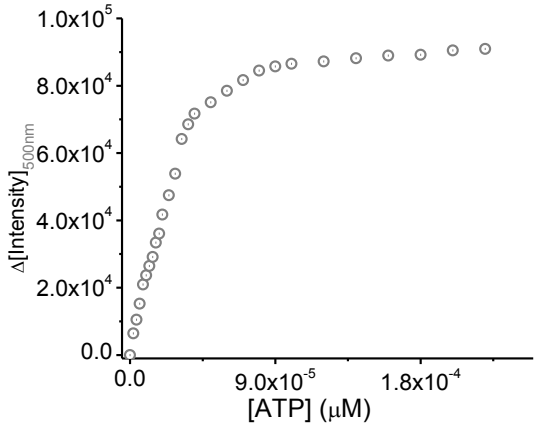

Figure 2. A plot of change in luminescence intensity at 500 nm recorded for a solution of L•Zn(II) (1.0 μM) with subsequent changes in [ATP] (0 – 10 μM) in 50 mM of aq. HEPES buffer solution having10 mM NaCl, 1 mM $MgCl_2$ (pH = 7.4, 25 °C, λ_{Ext} = 400 nm).

Binding of ATP to the Zn(II)-centre of L•Zn(II) was further confirmed by ^{31}P NMR spectral studies. Upfield shifts in the ^{31}P signals of the α- (1.84 ppm), β- (3.92 ppm) and γ- (2.39 ppm) of the phosphorus atoms of ATP bound to L•Zn(II) were observed (Figure 1). These shifts signify the binding to Zn-atom of L•Zn(II) through an oxygen atom containing the negative charge of the three conjugated phosphate units. This lead to the formation of a hepta-coordinated Zn(II)-centre in L•Zn(II) in presence of ATP (Scheme 2). Analogous ^{31}P NMR studies with ADP, showed shifts of 2.09 and 1.81 ppm for two P-atoms of ADP and this confirmed formation of a penta-coordinated Zn(II)-centre in L•Zn(II) (Figure S3).

The probe molecule L•Zn(II) shows a relatively large Stokes shift of ~100 nm, a highly desirable property for improved luminescence responses as it helps to reduce self-absorption and background noise as it leads to less interference from endogenous fluorophores. Systematic changes in the luminescence spectra as a function of varying [ATP] and [ADP] (0 to 100-mole equivalent) in HEPES buffer were recorded (Figures 2 (for ATP) and Figure S4 (for ADP)). A linear increase in luminescence intensity was observed until the [ATP] or [ADP] was 5 μM and a lower detection limit was evaluated as 8.4×10^{-9} MM for ATP and 1.25×10^{-8} M for ADP, respectively using the 3σ method (Figure S5). This also confirmed the high sensitivity of the chemodosimetric probe L•Zn(II) towards these NPPs.

The luminescence responses of L•Zn(II) (10 μM) were recorded after incubating with 100 mole equivalent of ATP/ADP (recorded after 20 min) in the absence and presence of large excess (1000 mole equiv.) of other anionic analytes / amino acids/ biomolecules (Figure S6). No further change in luminescence intensity was observed when spectra were recorded in the presence of all other possible competing anions/amino acids/ biomolecules. This clearly nullified any interference with other competing amino acids and biomolecules and confirmed the desired specificity of L•Zn(II) towards ATP/ ADP.

A short response time is also a very important criterion for developing an analytical reagent for quantitative estimation of biomarkers for any practical application.[41-42] To determine the response time of the probe L•Zn(II) towards ATP/ADP, luminescence intensities as a function of time in the absence and presence of ATP or ADP were monitored at 500 nm (λ_{Ext} = 400 nm). Although no detectable change in luminescence intensity with time was observed in the absence of ATP/ADP (Figure S7), the increase in luminescence intensity on addition of ATP or ADP, took ~3.8 min to plateau.

MTT assays were performed to check the cytotoxicity of the reagent towards RAW 264.7 macrophage cells. No decrease below 99% in cell viability was observed even after exposures to all tested concentrations of L•Zn(II) for 24 h (Figure S8). This confirmed the biocompatibility and the benign nature of the reagent L•Zn(II) towards live cells like RAW 264.7 macrophage cells. Thus, the reagent L•Zn(II) was ideally suited for application as an imaging reagent.

Widefield fluorescence microscopic images of RAW 264.7 macrophage cells after incubation with the reagent L•Zn(II) revealed that intracellular luminescence was almost entirely localized in the cytoplasmic region (Figure 3). Additionally, increases in [L•Zn(II)] resulted in a concomitant increase in intracellular emission. This was also evident in intensity maps generated from these data (Figure S9), which revealed the punctated nature of the images, indicating that L•Zn(II) was localized in specific regions of the cytoplasm. This was investigated in detail through co-localization studies using SIM.

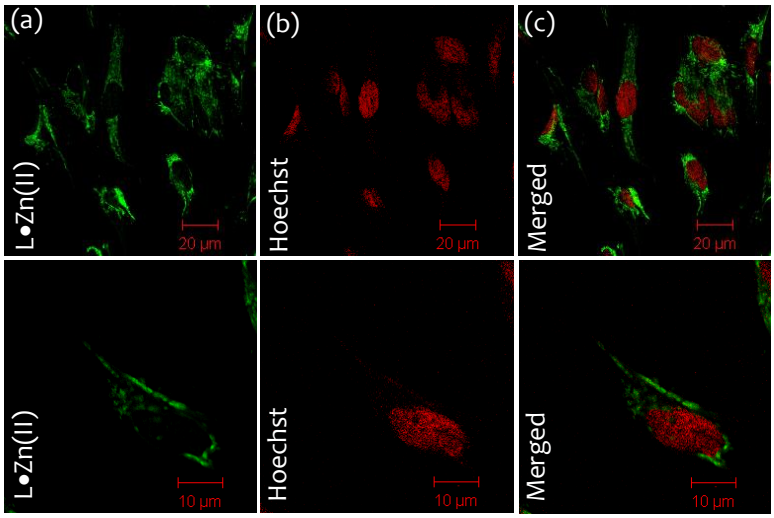

Figure 3. Confocal microscopy images of intracellular uptake of L•Zn(II) using Hoechst33342: confocal microscopy images of in cellulo emission of L•Zn(II) (panel a) with expansion shown underneath. Emission from Hoechst33342 (panel b) and the expansion of the same is shown below. The overlap of the intensity is shown in panel c and with expansion shown underneath. panel c shows the overlap of the green and red fluorescence, indicating intracellular green luminescence was almost entirely localized in the cytoplasmic region. λ_{Ext} = 400 nm.

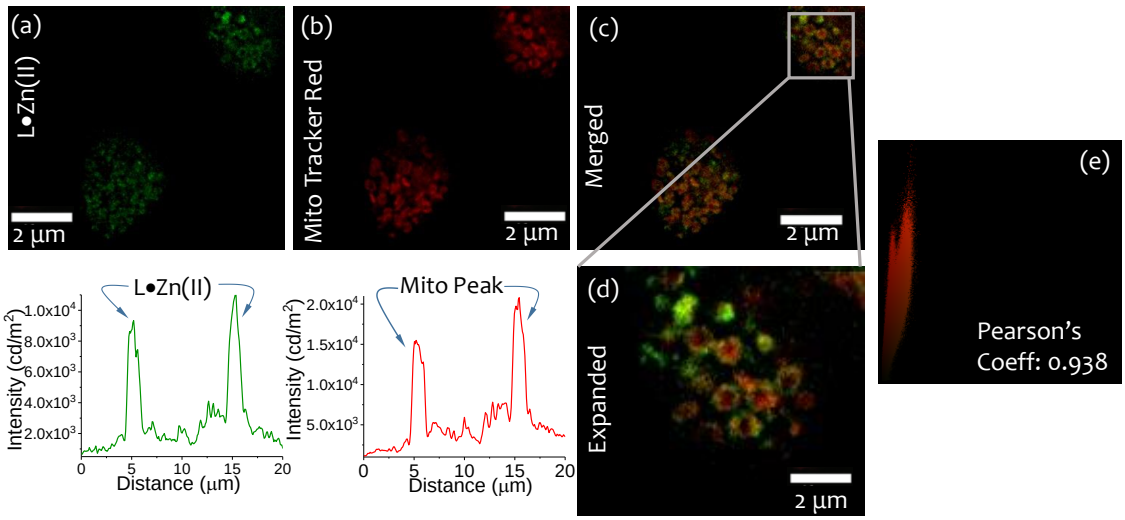

Figure 4. Colocalization experiments of intracellular localization of L•Zn(II) using MitoTracker probes: Widefield microscopy images of in cellular emission of L•Zn(II) (panel a) with intensity along the traced line shown underneath. Emission from Mito Tracker Deep Red (panel b) and intensity along the same line shown below. The overlap of the intensity is shown in panel c and its expansion in panel d. Panel c shows the overlap of

the green and red fluorescence, indicating mitochondria localization of L•Zn(II). Panel e shows the Pearson coefficient = 0.92. Scale bar 2 μm.

It is reported that the negative membrane potential of the mitochondrial inner membrane favors the accumulation of positively charged compounds in the mitochondrial matrix against their concentration gradient. [27, 43] Thus, the cationic nature of probe L•Zn(II) is expected to favor its accumulation in mitochondria.[44] To ascertain this hypothesis, colocalization studies were performed with Mito Tracker Deep Red (MTDR). The spectral properties of MTDR are complementary to that of L•Zn(II): L•Zn(II) is excited at 400 nm and its emission is collected at 500 to 550 nm, whereas MTDR is excited at 644 nm and emits at 655 nm (Figure 4).

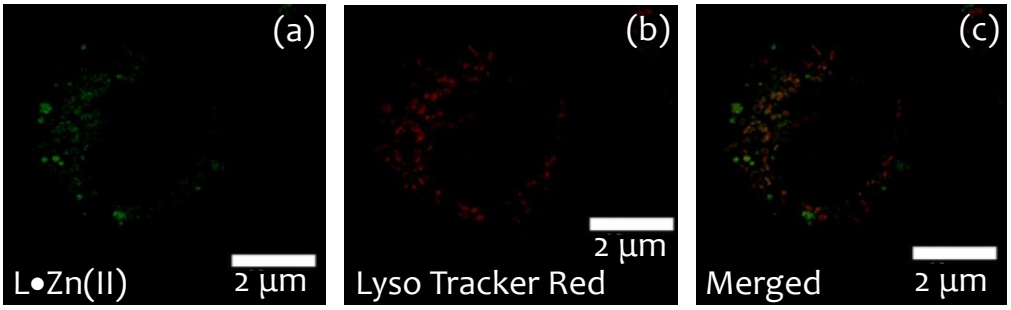

Figure 5. Colocalization experiments of intracellular localization of L•Zn(II) using Lyso Tracker probes: Widefield microscopy images of in cellular emission of L•Zn(II) (panel a) and emission from Lyso Tracker Deep Red (panel b). The overlap of the intensity is shown in panel c. Panel c shows no overlap of the green and red fluorescence indicates that L•Zn(II)is not localized over lysosomes. Scale bar 2 μm.

The intensity profile of the widefield images indicates that 60 percent of the MTDR signal matches that of L•Zn(II) (Figure 4). Calculated Pearson's coefficient (93%) also confirmed that L•Zn(II) localizes in the mitochondria of RAW cells (Fig. 3 and 3d). For further confirmation of subcellular localization, similar colocalization experiments were performed using Lyso Tracker Deep Red (LTDR) and Hoechst 33258. (Figures 5 and 6). These studies

ensured that L•Zn(II) does not localize in lysosomes or nuclei. This confirmed that L•Zn(II) exclusively localizes in the mitochondrial region of RAW 264.7 macrophage cells.

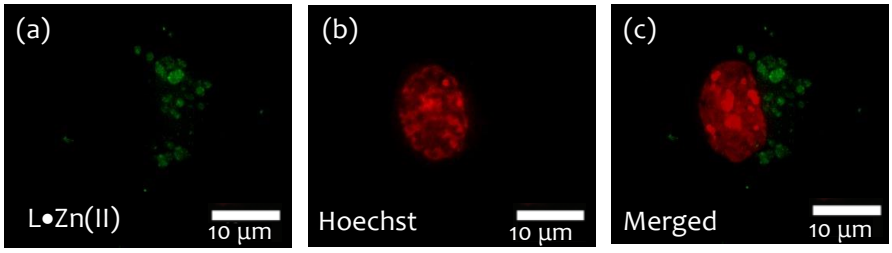

Figure 6. Dual colour SIM using L•Zn(II) in presence of Hoechst33342. Scale bar 10µm. (a) with L•Zn(II); (b) with Hoechst33342 and (c) is the overlap image. λ_{Ext} = 400 nm and scale bar 10µm.

After confirming the subcellular localization and specific recognition properties of L•Zn(II) *in-vitro* condition, its ability to detect NPPs in mitochondria of live cells was evaluated. The most abundant NPP inside the mitochondria is ATP. The reported normal concentration is ~2-3 mM in healthy mammalian cells, which is at least 5-times higher than those of other NPPs, excluding ADP (~0.7 mM). [45-46] Therefore, L•Zn(II) complex was used to detect changes in [ATP] within mitochondria during drug-induced apoptosis. Staurosporine (STS) an indolocarbazole is known to be a potent protein kinase C inhibitor [47-48] that enhances the ATP concentration in human cells. RAW 264.7 macrophage cell lines were incubated with STS (5 µM) and then these pre-treated cell lines were further treated with L•Zn(II). A distinct growth in luminescence intensity was observed in the mitochondria. Time-lapse images recorded in the presence of STS revealed a steady increase in intracellular luminescence intensity over 200 min (Figure 7 a-d). However, insignificant changes in luminescence intensity were observed in time-lapse images recorded for analogous experiments performed in the absence of STS (Figure S10). These results confirmed that the reagent L•Zn(II) can detect subtle changes in [ATP] or [ATP] + [ADP] in mitochondria for a period of 210 min during the pre-apoptotic stage (~3.5hr). This finding is consistent with

a previously reported result, which indicated that during STS-induced cell death the concentration of ATP in the cytosol gradually increases. [49-50]

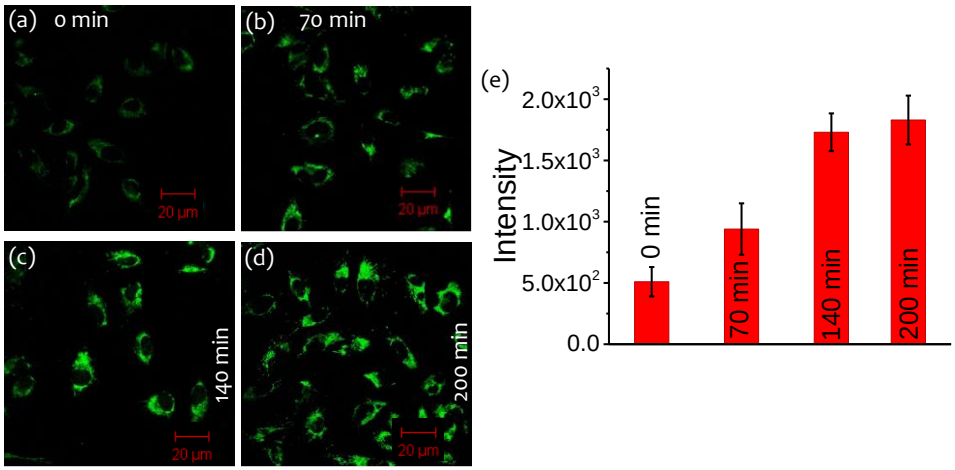

Figure 7. Fluorescence analysis of RAW 264.7 macrophage cells stained with L•Zn(II)complex. (a-d)Time-lapse confocal micrographs of RAW 264.7 macrophage cells stained with 1μM L•Zn(II)complex before (0 min) and after (200 min) treatment with 5 μM STS. Scale bars: 20 μm. (e) Time dependence of the change in fluorescence intensity upon treatment with 5 μM STS. Data represent the mean ± standard deviation of three replicates.

4. CONCLUSION

A new Zn(II)-based coordination complex was synthesized. This was found to bind specifically to NPPs in the presence of all other competing anions and natural amino acids. A significant enhancement in emission intensity was observed on the binding of NNPs to Zn(II)-centre of the L•Zn(II). This along with ^{1}H NMR spectroscopic studies were performed in confirming the binding affinities as well as the binding of the di- or tri-phosphate units of ADP or ATP to the Zn(II)-centre. This reagent was found to be physiologically benign. Structured illumination microscopic studies confirmed localization of the reagent in the mitochondrial region of the RAW 264.7 macrophage cells. This reagent could be utilized for probing the change in ATP concentration in mitochondria during drug-induced apoptosis. In addition, this

mitochondria targeting reagent may offer application in the study of intracellular transport mechanisms and mitochondrial dysfunction based diseases. Using such systems, *in-vivo* imaging technologies for live monitoring of various biological process will be possible.

ASSOCIATED CONTENT

Supporting Information:

The Supporting Information is available free of charge on the ACS Publications website at DOI: 10.xxxx/acs.cgd.xxxxxxx.

AUTHOR INFORMATION

Corresponding Author

Email: sumitpramanik@csmcri.res.in

James.thomas@sheffield.ac.uk

a.das@csmcri.res.in

Notes

The authors declare no competing financial interest.

ACKNOWLEDGMENTS

AD acknowledges SERB grants (EMR/2016/001850 & JCB/2017/000004) and DBT (India) grant BT/PR22251/NNT/ 28/1274/2017) for financial support. SKP acknowledges SERB (PDF/2015/000745) for financial support. SS acknowledges MRC Grant for Doctoral Fellowship.

REFERENCES

1. Zhou, Y.; Xu, Z.; Yoon, J., Fluorescent and colorimetric chemosensors for detection of nucleotides, FAD and NADH: highlighted research during 2004–2010. *Chemical Society Reviews* **2011,** *40* (5), 2222-2235.
2. Park, J., The Cell: A Molecular Approach, Second Edition. *The Yale Journal of Biology and Medicine* **2001,** *74* (5), 361-361.
3. Gourine, A. V.; Llaudet, E.; Dale, N.; Spyer, K. M., ATP is a mediator of chemosensory transduction in the central nervous system. *Nature* **2005,** *436*, 108.
4. Quail, D. F.; Joyce, J. A., Microenvironmental regulation of tumor progression and metastasis. *Nature Medicine* **2013,** *19*, 1423.
5. Fields, R. D.; Burnstock, G., Purinergic signalling in neuron–glia interactions. *Nature Reviews Neuroscience* **2006,** *7*, 423.
6. Hegg, C. C.; Greenwood, D.; Huang, W.; Han, P.; Lucero, M. T., Activation of Purinergic Receptor Subtypes Modulates Odor Sensitivity. *The Journal of Neuroscience* **2003,** *23* (23), 8291-8301.
7. Iorio, P. D.; Ballerini, P.; Caciagli, F.; Ciccarelli, R., PURINOCEPTOR-MEDIATED MODULATION OF PURINE AND NEUROTRANSMITTER RELEASE FROM NERVOUS TISSUE. *Pharmacological Research* **1998,** *37* (3), 169-178.
8. Ardito, F.; Giuliani, M.; Perrone, D.; Troiano, G.; Muzio, L. L., The crucial role of protein phosphorylation in cell signaling and its use as targeted therapy (Review). *International Journal of Molecular Medicine* **2017,** *40* (2), 271-280.
9. Wang, Z.; Cole, P. A., Chapter One - Catalytic Mechanisms and Regulation of Protein Kinases. In *Methods in Enzymology*, Shokat, K. M., Ed. Academic Press: 2014; Vol. 548, pp 1-21.
10. (a) Yegutkin, G. G., Nucleotide- and nucleoside-converting ectoenzymes: Important modulators of purinergic signalling cascade. *Biochimica et Biophysica Acta (BBA) - Molecular Cell Research* **2008,** *1783* (5), 673-694; Li, H.Y.; (b) Dai, L.J.; Quamme, G.A.; Effect of chemical hypoxia on intracellular ATP and cytosolic Mg^{2+} levels. J. Lab. Clin. Med. 1993 Sep;122(3):260-72; (c) Kurutas, E. B.; The importance of antioxidants which play the role in cellular response against oxidative/nitrosative stress: current state; Nutrition Journal, 201615:71; https://doi.org/10.1186/s12937-016-0186-5.
11. Burnstock, G., Purinergic signalling. *British Journal of Pharmacology* **2006,** *147* (Suppl 1), S172-S181.
12. Burnstock, G., Purinergic signalling: from discovery to current developments. *Experimental Physiology* **2014,** *99* (1), 16-34.
13. Hinkle, P. C.; Kumar, M. A.; Resetar, A.; Harris, D. L.; Mechanistic stoichiometry of mitochondrial oxidative phosphorylation. *Biochemistry* **1991,** *30* (14), 3576-3582.
14. Mookerjee, S. A.; Gerencser, A. A.; Nicholls, D. G.; Brand, M. D., Quantifying intracellular rates of glycolytic and oxidative ATP production and consumption using extracellular flux measurements. *Journal of Biological Chemistry* **2017,** *292* (17), 7189-7207.
15. Childress, E. S.; Alexopoulos, S. J.; Hoehn, K. L.; Santos, W. L., Small Molecule Mitochondrial Uncouplers and Their Therapeutic Potential. *Journal of Medicinal Chemistry* **2018,** *61* (11), 4641-4655.
16. Billker, O.; Lourido, S.; Sibley, L. D., Calcium-Dependent Signaling and Kinases in Apicomplexan Parasites. *Cell Host & Microbe* **2009,** *5* (6), 612-622.
17. Uzman, A., Molecular Cell Biology (4th edition) Harvey Lodish, Arnold Berk, S. Lawrence Zipursky, Paul Matsudaira, David Baltimore and James Darnell; Freeman & Co.,

New York, NY, 2000, 1084 pp., list price $102.25, ISBN 0-7167-3136-3. *Biochemistry and Molecular Biology Education* **2001,** *29* (3), 126-128.
18. Tan, K.-Y.; Li, C.-Y.; Li, Y.-F.; Fei, J.; Yang, B.; Fu, Y.-J.; Li, F., Real-Time Monitoring ATP in Mitochondrion of Living Cells: A Specific Fluorescent Probe for ATP by Dual Recognition Sites. *Analytical Chemistry* **2017,** *89* (3), 1749-1756.
19. Jung, S. H.; Kim, K. Y.; Lee, J. H.; Moon, C. J.; Han, N. S.; Park, S.-J.; Kang, D.; Song, J. K.; Lee, S. S.; Choi, M. Y.; Jaworski, J.; Jung, J. H., Self-Assembled Tb3+ Complex Probe for Quantitative Analysis of ATP during Its Enzymatic Hydrolysis via Time-Resolved Luminescence in Vitro and in Vivo. *ACS Applied Materials & Interfaces* **2017,** *9* (1), 722-729.
20. Singh, A.; Raj, P.; Dubowski, J. J.; Singh, N., ATP Induced Modulation in π–π Stacking Interactions in Pyrene Based Zinc Complexes: Chemosensor Study and Quantitative Investigation of Apyrase Activity. *Crystal Growth & Design* **2018,** *18* (8), 4320-4333.
21. Jose, D. A.; Mishra, S.; Ghosh, A.; Shrivastav, A.; Mishra, S. K.; Das, A., Colorimetric Sensor for ATP in Aqueous Solution. *Organic Letters* **2007,** *9* (10), 1979-1982.
22. Mahato, P.; Ghosh, A.; Mishra, S. K.; Shrivastav, A.; Mishra, S.; Das, A., Zn(II) based colorimetric sensor for ATP and its use as a viable staining agent in pure aqueous media of pH 7.2. *Chemical Communications* **2010,** *46* (48), 9134-9136.
23. Ahmad, H.; Hazel, B. W.; Meijer, A. J. H. M.; Thomas, J. A.; Wilkinson, K. A., A Self-Assembled Luminescent Host That Selectively Senses ATP in Water. *Chemistry – A European Journal* **2013,** *19* (16), 5081-5087.
24. Yu, H.; Zhang, X.; Xiao, Y.; Zou, W.; Wang, L.; Jin, L., Targetable Fluorescent Probe for Monitoring Exogenous and Endogenous NO in Mitochondria of Living Cells. *Analytical Chemistry* **2013,** *85* (15), 7076-7084.
25. Li, J.; Kwon, N.; Jeong, Y.; Lee, S.; Kim, G.; Yoon, J., Aggregation-Induced Fluorescence Probe for Monitoring Membrane Potential Changes in Mitochondria. *ACS Applied Materials & Interfaces* **2018,** *10* (15), 12150-12154.
26. Xu, Z.; Xu, L., Fluorescent probes for the selective detection of chemical species inside mitochondria. *Chemical Communications* **2016,** *52* (6), 1094-1119.
27. Pramanik, S. K.; Sreedharan, S.; Singh, H.; Khan, M.; Tiwari, K.; Shiras, A.; Smythe, C.; Thomas, J. A.; Das, A., Mitochondria Targeting Non-Isocyanate-Based Polyurethane Nanocapsules for Enzyme-Triggered Drug Release. *Bioconjugate Chemistry* **2018**.
28. Han, Y.; Li, M.; Qiu, F.; Zhang, M.; Zhang, Y.-H., Cell-permeable organic fluorescent probes for live-cell long-term super-resolution imaging reveal lysosome-mitochondrion interactions. *Nature Communications* **2017,** *8* (1), 1307.
29. Huang, B.; Babcock, H.; Zhuang, X., Breaking the Diffraction Barrier: Super-Resolution Imaging of Cells. *Cell* **2010,** *143* (7), 1047-1058.
30. Hauser, M.; Wojcik, M.; Kim, D.; Mahmoudi, M.; Li, W.; Xu, K., Correlative Super-Resolution Microscopy: New Dimensions and New Opportunities. *Chemical Reviews* **2017,** *117* (11), 7428-7456.
31. Stone, M. B.; Shelby, S. A.; Veatch, S. L., Super-Resolution Microscopy: Shedding Light on the Cellular Plasma Membrane. *Chemical Reviews* **2017,** *117* (11), 7457-7477.
32. Moon, S.; Yan, R.; Kenny, S. J.; Shyu, Y.; Xiang, L.; Li, W.; Xu, K., Spectrally Resolved, Functional Super-Resolution Microscopy Reveals Nanoscale Compositional Heterogeneity in Live-Cell Membranes. *Journal of the American Chemical Society* **2017,** *139* (32), 10944-10947.
33. Sreedharan, S.; Gill, M. R.; Garcia, E.; Saeed, H. K.; Robinson, D.; Byrne, A.; Cadby, A.; Keyes, T. E.; Smythe, C.; Pellett, P.; Bernardino de la Serna, J.; Thomas, J. A., Multimodal Super-resolution Optical Microscopy Using a Transition-Metal-Based Probe Provides Unprecedented Capabilities for Imaging Both Nuclear Chromatin and Mitochondria. *Journal of the American Chemical Society* **2017,** *139* (44), 15907-15913.

34. Kovacs, D.; Lu, X.; Mészáros, L. S.; Ott, M.; Andres, J.; Borbas, K. E., Photophysics of Coumarin and Carbostyril-Sensitized Luminescent Lanthanide Complexes: Implications for Complex Design in Multiplex Detection. *Journal of the American Chemical Society* **2017,** *139* (16), 5756-5767.
35. Pedone, A.; Gambuzzi, E.; Barone, V.; Bonacchi, S.; Genovese, D.; Rampazzo, E.; Prodi, L.; Montalti, M., Understanding the photophysical properties of coumarin-based Pluronic–silica (PluS) nanoparticles by means of time-resolved emission spectroscopy and accurate TDDFT/stochastic calculations. *Physical Chemistry Chemical Physics* **2013,** *15* (29), 12360-12372.
36. Francesconi, O.; Gentili, M.; Bartoli, F.; Bencini, A.; Conti, L.; Giorgi, C.; Roelens, S., Phosphate binding by a novel Zn(ii) complex featuring a trans-1,2-diaminocyclohexane ligand. Effective anion recognition in water. *Organic & Biomolecular Chemistry* **2015,** *13* (6), 1860-1868.
37. Das, P.; Ghosh, A.; Kesharwani, M. K.; Ramu, V.; Ganguly, B.; Das, A., ZnII–2,2′:6′,2″-Terpyridine-Based Complex as Fluorescent Chemosensor for PPi, AMP and ADP. *European Journal of Inorganic Chemistry* **2011,** *2011* (20), 3050-3058.
38. Ghosh, A.; Shrivastav, A.; Jose, D. A.; Mishra, S. K.; Chandrakanth, C. K.; Mishra, S.; Das, A., Colorimetric Sensor for Triphosphates and Their Application as a Viable Staining Agent for Prokaryotes and Eukaryotes. *Analytical Chemistry* **2008,** *80* (14), 5312-5319.
39. Das, P.; Bhattacharya, S.; Mishra, S.; Das, A., Zn(ii) and Cd(ii)-based complexes for probing the enzymatic hydrolysis of Na4P2O7 by alkaline phosphatase in physiological conditions. *Chemical Communications* **2011,** *47* (28), 8118-8120.
40. Das, P.; Chandar, N. B.; Chourey, S.; Agarwalla, H.; Ganguly, B.; Das, A., Role of Metal Ion in Specific Recognition of Pyrophosphate Ion under Physiological Conditions and Hydrolysis of the Phosphoester Linkage by Alkaline Phosphatase. *Inorganic Chemistry* **2013,** *52* (19), 11034-11041.
41. Masucci, G. V.; Cesano, A.; Hawtin, R.; Janetzki, S.; Zhang, J.; Kirsch, I.; Dobbin, K. K.; Alvarez, J.; Robbins, P. B.; Selvan, S. R.; Streicher, H. Z.; Butterfield, L. H.; Thurin, M., Validation of biomarkers to predict response to immunotherapy in cancer: Volume I — pre-analytical and analytical validation. *Journal for Immunotherapy of Cancer* **2016,** *4*, 76.
42. Agarwalla, H.; Anila, H. A.; Ali, F.; Pradhan, S. R.; Ganguly, B.; Pramanik, S. K.; Das, A., Fluorescent chemodosimeter for quantification of cystathionine-γ-synthase activity in plant extracts and imaging of endogenous biothiols. *Chemical Communications* **2018,** *54* (65), 9079-9082.
43. Liu, X.-L.; Niu, L.-Y.; Chen, Y.-Z.; Zheng, M.-L.; Yang, Y.; Yang, Q.-Z., A mitochondria-targeting fluorescent probe for the selective detection of glutathione in living cells. *Organic & Biomolecular Chemistry* **2017,** *15* (5), 1072-1075.
44. Zielonka, J.; Joseph, J.; Sikora, A.; Hardy, M.; Ouari, O.; Vasquez-Vivar, J.; Cheng, G.; Lopez, M.; Kalyanaraman, B., Mitochondria-Targeted Triphenylphosphonium-Based Compounds: Syntheses, Mechanisms of Action, and Therapeutic and Diagnostic Applications. *Chemical Reviews* **2017,** *117* (15), 10043-10120.
45. Traut, T. W., Physiological concentrations of purines and pyrimidines. *Molecular and Cellular Biochemistry* **1994,** *140* (1), 1-22.
46. Barshop, B. A.; Adamson, D. T.; Vellom, D. C.; Rosen, F.; Epstein, B. L.; Seegmiller, J. E., Luminescent immobilized enzyme test systems for inorganic pyrophosphate: Assays using firefly luciferase and nicotinamide-mononucleotide adenylyl transferase or adenosine-5′-triphosphate sulfurylase. *Analytical Biochemistry* **1991,** *197* (1), 266-272.
47. Wu-Zhang, A. X.; Newton, A. C., Protein Kinase C Pharmacology: Refining the Toolbox. *The Biochemical journal* **2013,** *452* (2), 195-209.

48. Tamaoki, T.; Nakano, H., Potent and Specific Inhibitors of Protein Kinase C of Microbial Origin. *Bio/Technology* **1990,** *8*, 732.
49. Atlante, A.; Giannattasio, S.; Bobba, A.; Gagliardi, S.; Petragallo, V.; Calissano, P.; Marra, E.; Passarella, S., An increase in the ATP levels occurs in cerebellar granule cells en route to apoptosis in which ATP derives from both oxidative phosphorylation and anaerobic glycolysis. *Biochimica et Biophysica Acta (BBA) - Bioenergetics* **2005,** *1708* (1), 50-62.
50. Celsi, F.; Pizzo, P.; Brini, M.; Leo, S.; Fotino, C.; Pinton, P.; Rizzuto, R., Mitochondria, calcium and cell death: A deadly triad in neurodegeneration. *Biochimica et Biophysica Acta (BBA) - Bioenergetics* **2009,** *1787* (5), 335-344.

TOC

A Fluorescent Chemodosimeter for Organelle-Specific Imaging of Nucleoside Polyphosphate Dynamics in Living Cells

Harwinder Singh, Sreejesh Sreedharan, Rajeswari Tiwari, Christa Walther, Carl Smythe, Sumit Kumar Pramanik, Jim. A. Thomas and Amitava Das

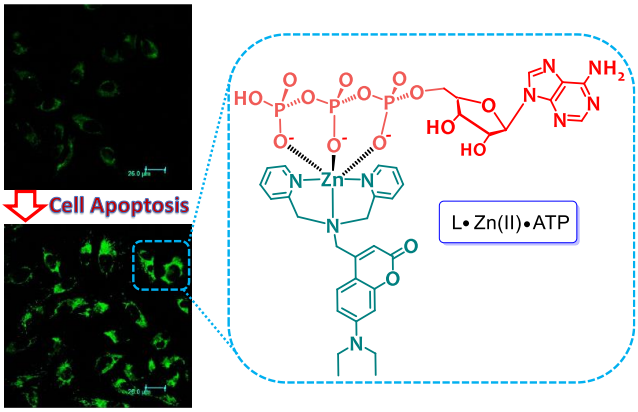

New fluorescence-based reagent for probing subtle changes of NPPs in mitochondria